Electronic Supplementary Information

Protein-free Ribosomal RNA folds to a near-native state in the presence of Mg^{2+}

Timothy K. Lenz, Ashlyn M. Norris, Nicholas V. Hud and Loren Dean Williams *

Department of Chemistry & Biochemistry, Georgia Institute of Technology, Atlanta, GA, 30332, United States

Production of *T. thermophilus* LSU rRNA

T. thermophilus LSU rRNA was produced by *in vitro* transcriptions using previously described constructs and protocols.[1] The rRNA was purified to remove salts.[2,3] The purified RNA yields a single tight band on denaturing PAGE gel (SequaGel UreaGel System, National Diagnostics, Figure S1).

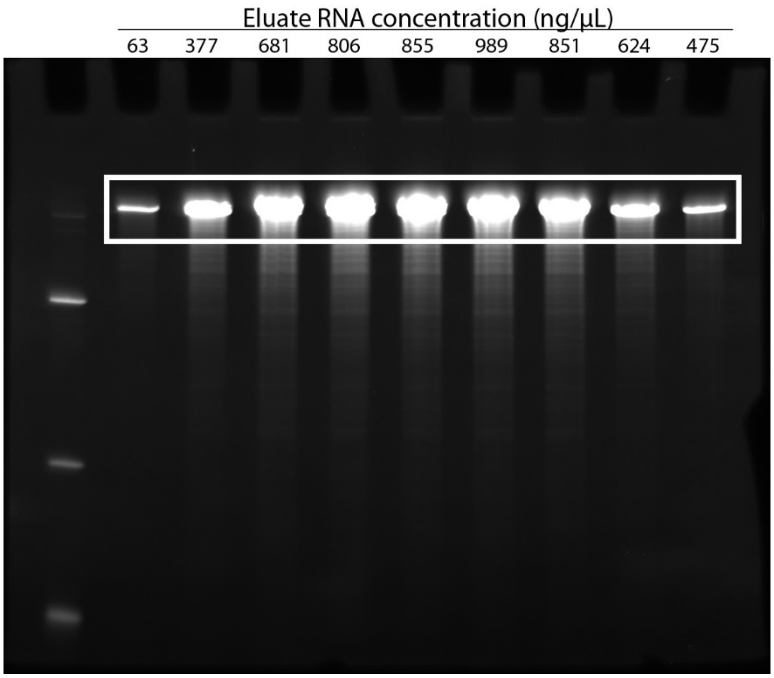

Figure S1. Denaturing PAGE gel of purified, *in vitro*-transcribed LSU rRNA. Equal volumes of eluate were loaded in each lane. RNA concentrations of each sequential eluate fraction are indicated, as determined by absorbance at 260 nm. The white box highlights the bands representing LSU rRNA.

NMIA modification of *T. thermophilus* LSU rRNA

SHAPE exploits the variable susceptibly of the 2'-hydroxyl group to attack by electrophiles such as NMIA (*N*-methylisatoic anhydride). Reactivity to NMIA is modulated by the interatomic distance between the 2'-OH and non-bridging phosphate oxygen (PO), and is commensurate with local RNA flexibility. Generally, nucleotides that are constrained by canonical cis Watson-Crick/Watson-Crick (cWW) base pairing exhibit low reactivity toward SHAPE reagents, while nucleotides that participate in non-canonical or unusual RNA-RNA interactions exhibit variable reactivity, and flexible unpaired nucleotides are highly SHAPE reactive. Final conditions in SHAPE modification reactions were 400 nM *in vitro*-transcribed rRNA strand, 6.5 mM NMIA, 200 mM NaOAc, 50 mM NaHEPES, pH 8 and either 1 mM 1,2-diaminocyclohexanetetraacetic acid (DCTA) or 10 mM $MgCl_2$ in a total volume of 440 µL.

Lyophilized RNA was rehydrated with nuclease-free water and RNA was refolded by heating to 60 ^{o}C for 30 s followed by equilibration at room temperature. DCTA, a high-affinity chelator of divalent cations, was included in Na^+ samples to ensure absence of contaminating divalent cations in solution, providing a 'divalent-free RNA' baseline reading. Folded RNA samples were divided equally into SHAPE modification and background control reactions. NMIA in anhydrous DMSO was added to SHAPE reactions, and anhydrous DMSO alone was added to control reactions. rRNA modification reactions were carried out at 37 ^{o}C for 1 h. Divalent cations were removed from samples by mixing with Chelex 100 resin (Bio-Rad) followed by centrifugation through 0.22 µm filters. RNA was purified from reaction mixtures via sodium acetate precipitation, and pellets were resuspended in TE buffer (10 mM Tris-HCl, 1 mM EDTA, pH 8.0). RNA recovery was >80%.

Reverse Transcription of NMIA-modified *T. thermophilus* LSU rRNA

NMIA-modified RNA solutions were divided equally into reactions with 11 different 5'-[6-FAM]-labeled DNA reverse transcription (RT) primers (Table S1). Primers were designed such that their 5' ends targeted non-helical regions of the LSU rRNA based on the secondary structure. Modified rRNA (20 µL) was added to 12 pmol of each primer in 15 µL of TE buffer. Primers were annealed to rRNA by heating to 95 °C for 30 s, incubation at 65 °C for 3 min, and then cooling to 4 °C. RT reactions (50 µL total) were assembled with 10 µL 5x Maxima RT Buffer (Thermo Scientific), a final dNTP concentration of 2.5 mM, and 200 U Maxima Reverse Transcriptase (Thermo Scientific). Reactions were incubated at 55 °C for 2 h and terminated by heat inactivation at 85 °C for 5 min. Parallel sequencing reactions for use in data processing were run with 3 pmol of unmodified RNA. RNA was sequenced by RT/chain termination with all four dideoxyNTPs (ddNTPs) at a ratio of 1:1 ddNTP to dNTP. A control reaction without ddNTPs was also prepared.

RT reaction mixtures (1 µL) were mixed with 0.3 µL of ROX-labeled DNA sizing ladder (for alignment of different traces) and 8.7 µL Hi-Di Formamide (Applied Biosystems) in a 96-well plate. Plates were heated at 95 °C for 5 min and resolved by capillary electrophoresis using a 3130 Genetic Analyzer (Applied Biosystems) at 65 °C with a custom fluorescence spectral calibration. The capillary array was loaded with Performance Optimized Polymer-4 (Applied Biosystems).

Table S1. Reverse transcription primers used in SHAPE.

Primer Sequence (5' -> 3')	Target region
AAGCTTGGAGGGGTCAAGACCTC	2891-2913[a]
GCCCGTGGCGGATAGAGAC	2608-2626
CCGACATCGAGGTGCCAAACCTCC	2486-2509
CCCGCCAAGCGCTGTC	2224-2239
GTTCAATTTCACCGGGTCCC	2002-2021
CGCGCCTGAGTGCTCTTG	1631-1647
CGTTACTCATGCCGGCATTCGC	1250-1271
CCTTAGCTGGCGGTCTC	987-1003
GCTATCTCCGGGCTCGG	790-806
CTTTTCACCTTTCCCTCACGG	461-481
CAGGGAGTCGATTTCTCTTTCC	219-240

[a]Native *T. thermophilus* LSU rRNA sequence ends at nucleotide 2902. Nucleotides 2903-2913 are remnants of cloning/*in vitro* transcription.

SHAPE data processing

Capillary electropherograms were converted into SHAPE reactivities using previously-described in-house MATLAB scripts.[1,4] In summary, data processing involves alignment of traces, baseline correction, peak detection and annotation, peak integration, decay correction and scaling, background subtraction, normalization, and averaging of data from multiple primers in regions with overlapping data. Reverse transcription provided reads ranging 200 to 600 nucleotides in length Overlapping data from independent primer reads were in very good agreement. In certain regions, two or three independent measures of the reactivity of a given nucleotide from different primer reads were averaged to yield a final SHAPE value. Processed SHAPE data were inspected for disagreement between overlapping regions from independent primer reads, and a small proportion of data was discarded based on these disagreements.

SHAPE data analysis

SHAPE data were collected for 2890 of the 2911 LSU rRNA nucleotides (>99%). Unless otherwise noted, results described below are consistent between Na^{+} and Na^{+}/Mg^{2+} conditions. Virtually all LSU rRNA predicted to be double-stranded by the canonical secondary structure appears double-stranded here in Na^{+}, as indicated by low SHAPE reactivity (<0.6). Less than 1% of internal helical nucleotides are SHAPE reactive. Regions of the canonical secondary structure that do not participate in local cWW base pairs (non-canonical base pairs, bulges, loops, and other unpaired nucleotides) exhibit variable reactivity as expected, with many nucleotides exhibiting moderate to high SHAPE reactivity (Table S2). Virtually all LSU rRNA nucleotides that exhibit moderate to high SHAPE reactivity (>0.6) are observed in loops, bulges, mismatches, or otherwise single-stranded regions of the canonical secondary structure. Examples of long canonical helices that display consistently low SHAPE reactivity can be found in Table S2. Many rRNA helices bear small bulges (1-3 nt), mismatches, and internal loops. These features exhibit moderate to high SHAPE reactivity (Table S2, Fig S2) but the flanking canonical base pairs still exhibit low SHAPE values. More often, helices bearing small non-canonical structures exhibit consistently low reactivity, even at the non-canonical positions (Table S2, Figure S2). Although these nucleotides may not be involved in local canonical base pairs, they are still constrained (by non-local or non-canonical interactions) in such a way as to be unreactive to SHAPE. Less than 10% of helices contain one or more expected helical nucleotides that exhibit moderate to high SHAPE reactivity (>0.6, Table S2).

Greater than half of reactive helical nucleotides are adjacent to non-canonical structures (bulges, mismatches, loops), which could induce increased mobility/flexibility of neighboring nucleotides. Prime examples of SHAPE reactive non-canonical regions are listed in Table S2, including helix-capping loops, internal loops/bulges, and intervening non-canonical regions between helices.

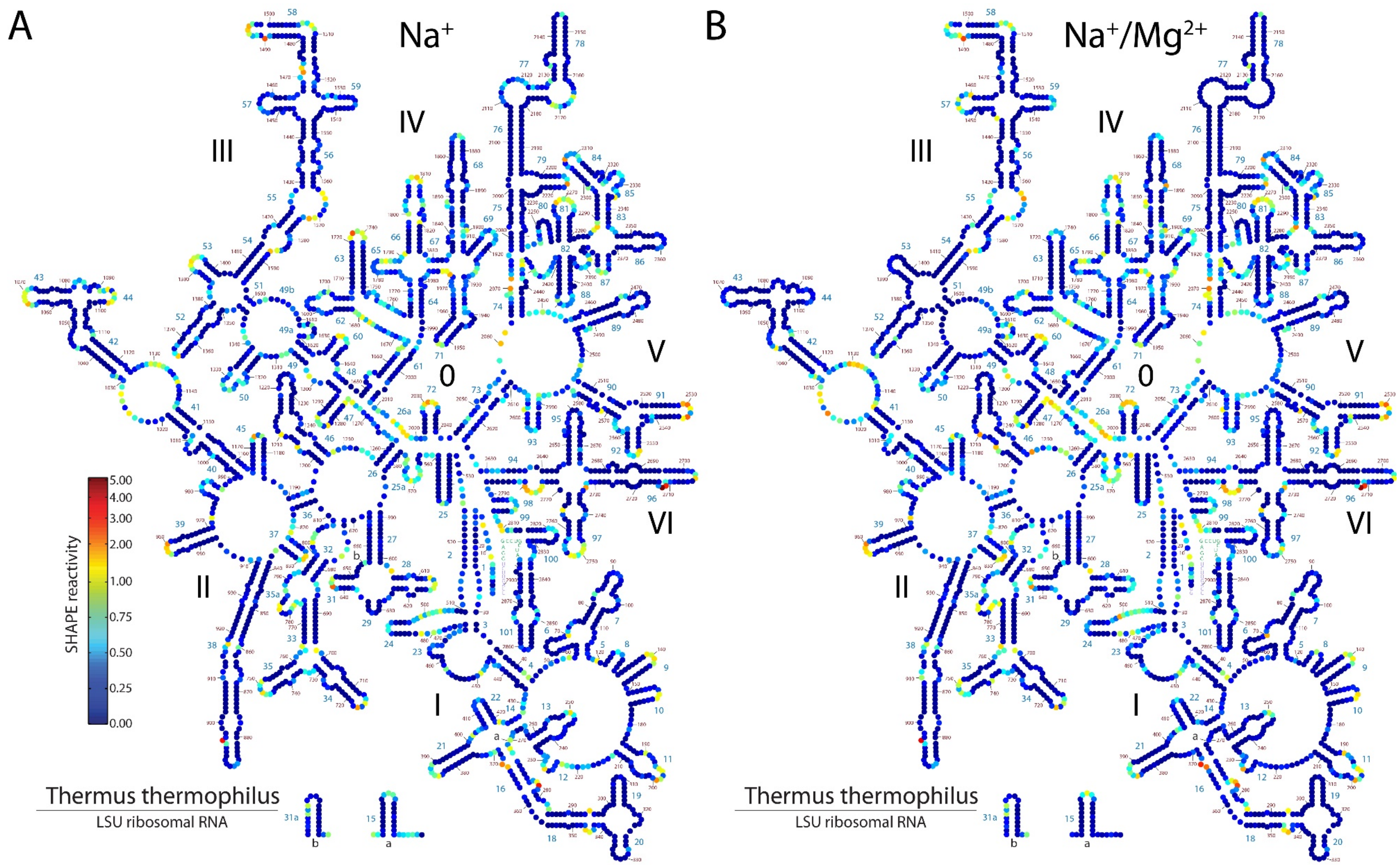
A
Na+
B
Na+/Mg2+
III
IV
V
VI
0
I
II
SHAPE reactivity
5.00
4.00
3.00
2.00
1.00
0.75
0.50
0.25
0.00
Thermus thermophilus
LSU ribosomal RNA

Figure S2. SHAPE reactivities for the *T. thermophilus* LSU rRNA. SHAPE reactivities are mapped onto LSU rRNA secondary structure in presence of A) *Na^+* or B) *Na^+/Mg^{2+}*. All samples contained 200 mM NaOAc, 50 mM NaHEPES, pH 8. Helix numbers (blue), domain numbers, and insertion points are indicated. Nucleotide numbers are denoted every ~10 nt (*E. coli* numbering). Regions where SHAPE data is not available (5' and 3' ends) are displayed as sequence only. This figure was generated with RiboVision.

Table S2: LSU rRNA helices exhibiting low vs. moderate/high SHAPE reactivity in both *Na^+* & *Na^+/Mg^{2+}*

Low SHAPE reactivity in *Na^+* & *Na^+/Mg^{2+}*		Helices bearing indicated features with moderate to high SHAPE reactivity in *Na^+* & *Na^+/Mg^{2+}*				
Long unreactive LSU rRNA helices	Helices bearing unreactive bulges, mismatches, or internal loops	Helix-capping loops	Internal loops/bulges	Inter-helical regions	Bulges, mismatches, or internal loops	Reactive helical nucleotides
2	2	9	16	41/42	18	1
21	7	31	18	55/56	38	4
25	13	34	38	61/62	62	31a
27	28	39	58	73/74	66	35a
33	34	66	96		68	47
42	35	72	98		89	65
54	39	81			90	67
63	41	91			91	73
76	50				93	74
	52				94	
	77				96	
	78					
	86					
	88					
	95					
	101					

In analysis of Mg^{2+}-dependent SHAPE changes, values >0.3 SHAPE units (positive or negative) are termed 'ΔMg^{2+} sites', i.e., sites which experience a significant Mg^{2+}-dependent alteration in SHAPE reactivity; ~7.5% of LSU rRNA nucleotides exceed this threshold. In presence of 10 mM Mg^{2+}, a larger proportion of the LSU rRNA (128 nt) becomes less reactive to SHAPE than exhibits increased reactivity (92 nt).

Of the >100 canonical helices found in the LSU rRNA, only three—H16, H77, and H83—contain internal ΔMg^{2+} sites not immediately adjacent to a non-canonical region. These sites all exhibit decreases in SHAPE reactivity consistent with formation/stabilization of a canonical base pairing. Three ΔMg^{2+} sites are found at guanine nucleotides of H16, in a short segment at the 5' end of the helix (positions 272B-272D). These nucleotides decrease significantly in SHAPE reactivity in presence of Mg^{2+}, indicating reduced flexibility/increased stability of the 5' end of H16. Single guanine residues near the 5' ends of H77 (G2121) and H83 (G2290) exhibit similarly decreased SHAPE reactivity in presence of Mg^{2+}, consistent with helix ends that are frayed in the absence of Mg^{2+} and stabilized in its presence.

ΔMg^{2+} sites are frequently found in helix-capping RNA loops. Many internal loops and bulges bear one or more ΔMg^{2+} sites. Substantial Mg^{2+}-dependent changes in SHAPE reactivity are also observed in inter-helical regions. A summary of LSU rRNA regions that bear ΔMg^{2+} sites is provided in Table S3. Loops that do not participate in RNA-RNA tertiary interactions within the assembled LSU exhibit ΔMg^{2+} values close to zero; counter-examples that meet this criterion include the loops that cap H15, H34, H45, H68, and H69 (Figure 1, S5). Most nucleotides in these loops experience little to no Mg^{2+}-dependent change in SHAPE reactivity, and those few nucleotides that do yield significant ΔMg^{2+} values exhibit decreases, suggesting local Mg^{2+}-induced stabilization of loop structures. H34, H68, and H69 are involved in intersubunit bridging interactions with the SSU *in vivo*.[5] In the experiments presented here only the LSU rRNA is present, and therefore these loops are not expected to form the intersubunit interactions found in the assembled ribosome.

Table S3: LSU helices exhibiting ΔMg^{2+} sites

Classification of ΔMg^{2+} site-bearing helices		
Helix-capping loops	Internal loops/bulges	Intervening non-canonical regions between helices
25	16	2/24
28	18	4/5
31	35	4/14
35	38	5/8
37	46	11/12
43	50	14/15
44	56	15/16
45	58	16/21
52	61	21/22
53	68	25/25a
57	74	26/46
58	96	41/42
59		49/50
60		49a/51
63		50/51
69		52/53
72		55/56
79		73/74
81		76/77
84		77/78
88		
91		
92		
97		

Helix 74

Canonical helix regions in H74 and its interaction partner H37 are marked by stretches of cWW base pairs (black lines, Figure 2B) and cross-strand base-stacking interactions (cyan lines). H74 exhibits three ΔMg^{2+} sites; A2060 decreases in SHAPE reactivity, while G2067 and U2068 increase in SHAPE reactivity. In the assembled LSU, A2060 is involved in several long-distance tertiary interactions: a base-sugar interaction between its primary amine and the 2'-OH of U807, and base-stacking interactions with U1255 and G2502. The ΔMg^{2+} data imply formation of one or more of these tertiary interactions, restraining A2060 and making it significantly less SHAPE reactive. The increased reactivity at G2067 and U2068 also suggests formation of nearby tertiary interactions. U2068 is a single nucleotide bulge, and G2067 neighbors the bulge. Neither U2068 nor G2067 are directly involved in long-range RNA-RNA tertiary interactions as classified by FR3D, but neighboring nucleotide G2609 participates in a base-sugar interaction with A676 in which the amine of A676 contacts the 2'-OH of G2609. U827 and G805 contain atoms within 5 Å of U2608, but not close enough to be classified as a direct interaction by the geometric pattern recognition used by FR3D. Indirect Mg^{2+}-induced formation of one or more of these tertiary interactions may cause U2068 to 'flip-out' of H74, into a conformation with a greater 2'-OH/PO interatomic distance, resulting in increased SHAPE reactivity. Higher reactivity at G2067 may be related to increased instability and strain caused by formation of tertiary interactions at positions U2068 or G2609. Nearby base-sugar tertiary interactions between the loop of H37 and G2445/G2446 may also influence SHAPE reactivity of G2067 and U2068.

uL1 protuberance

Within the uL1 protuberance, helical regions of H76 and H77 are marked by stretches of cWW base pairs and cross-strand base-stacking interactions (Figure 2D). Thirteen ΔMg^{2+} sites are found in the uL1 protuberance, all negative, indicating increased stability/decreased flexibility induced by Mg^{2+} (Table S4). These changes in SHAPE reactivity are consistent with formation of local tertiary interactions at or near the ΔMg^{2+} sites. Eight base-stacking tertiary interactions and two base-phosphate interactions are observed within the uL1 protuberance in the assembled LSU (Figure 2D, Table S4). All ΔMg^{2+} sites are at or near nucleotides involved in these local tertiary interactions, and are in agreement with formation of that interaction network. Two base-phosphate tertiary interactions occur within the uL1 protuberance; the primary amine group of G2165 contacts a PO of G2116, and the carbonyl group of G2125 contacts a PO of A2171. The 5' strand of the 5 base-pair H77 exhibits decreased SHAPE reactivity, supporting Mg^{2+}-induced stabilization (Figure 2D).

Table S4: ΔMg^{2+} sites and base-stacking interactions in the uL1 protuberance

Sites of Mg^{2+}-induced SHAPE reactivity decrease	Nucleotide pairs involved in base-stacking interactions[a]
U2113	G2110/G2120
A2114	C2111/U2118
A2117	G2116/A2171
U2118	A2119/A2170
A2119	A2119/A2169
G2121	C2128/U2172
G2165	G2162/U2172
G2166	G2166/A2170
U2167	
G2168	
A2170	
A2171	
U2172	

[a] Interactions defined by FR3D

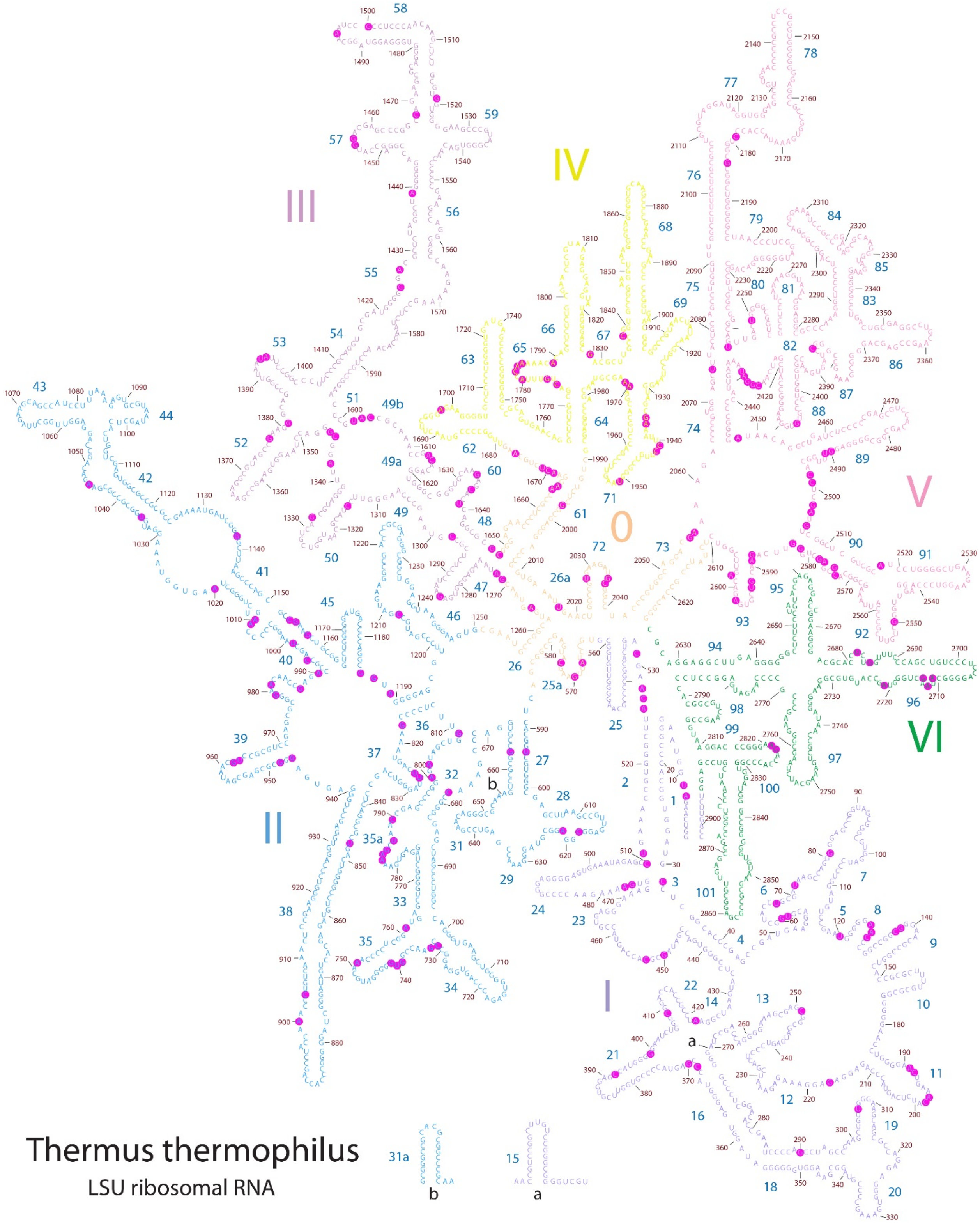

Thermus thermophilus
LSU ribosomal RNA

Figure S3. First-shell Mg^{2+} Interactions with the LSU rRNA from *T. thermophilus* as observed in the assembled ribosome. Magenta circles denote nucleotides that form first shell contacts with Mg^{2+} in the crystal structure of the *T. thermophilus* ribosome (PDB IDs: 2J00 and 2J01). Nucleotides are colored by domain. Nucleotide numbers are indicated every ~10 nt (*E. coli* numbering). Helix numbers (blue) and domain numbers are shown. This figure was generated with RiboVision.

Direct Mg^{2+}-rRNA interactions

Nucleotides that directly contact Mg^{2+} are dispersed throughout the secondary structure, in all seven domains of the LSU rRNA (Figure S3). In 3D, proportionate incidence of Mg^{2+} is highest close to the peptidyl transferase center (PTC) and decreases with increasing radial distance from the PTC.[6,7] Some ΔMg^{2+} sites are at or near direct Mg^{2+}-coordinating nucleotides, while a roughly equal proportion are distant in primary, secondary, and 3D structure from nucleotides expected to interact directly with Mg^{2+} (Figures 2 & S4). Conversely, a considerable proportion of nucleotides that bind Mg^{2+} in the assembled LSU are distant from ΔMg^{2+} sites, suggesting that Mg^{2+}-binding does not consistently translate to altered local SHAPE reactivity. Alternatively, some expected Mg^{2+}-binding sites may not be occupied under the studied conditions. ΔMg^{2+} sites that are distant from direct Mg^{2+}-coordination sites may be influenced by interactions with hydrated Mg^{2+}, loosely bound Mg^{2+} not observed in the 3D structure, or structurally-distant RNA-Mg^{2+} binding events that allow distal RNA regions to come into close proximity in 3D to form RNA-RNA tertiary interactions. In H74, a Mg^{2+} cation directly contacts a phosphate oxygen of G2502 in close proximity to several ΔMg^{2+} sites, but no Mg^{2+} cations coordinate directly with RNA at or near ΔMg^{2+} sites G2067 or U2068 (Figures 2A & 2B). Two Mg^{2+} cations are coordinated directly by the L1 protuberance, but none at or directly adjacent to ΔMg^{2+} sites (Figures 2C & 2D). Several hexahydrated Mg^{2+} cations interact in a specific manner with the uL1 protuberance, some at nucleotides involved in the loop-loop interaction. The Mg^{2+} effects observed in the uL1 protuberance are consistent with hydrated Mg^{2+} binding, structurally-distant RNA-Mg^{2+} binding events, or non-specific stabilization, not by direct Mg^{2+} coordination. Ultimately, tertiary structure formation and RNA-Mg^{2+} interactions are inextricably entangled, and it is virtually impossible to decouple the two, especially for large RNA structures such as the LSU rRNA.

Inter-domain interactions

The largest number of long-range inter-domain interactions in the assembled LSU is between DII and DV. We observe evidence consistent with Mg^{2+}-induced formation of 3 distinct sets of RNA-RNA interactions between DII/DV (Figures S4B & S4O, and Table S5). In the rRNA-Mg^{2+} state, all long-range inter-domain interactions observed in the assembled LSU are inferred between D0/DIII (Figure S4I), D0/DV (Figure S4V), DII/DVI (Figures S4T, S4Z), and DV/DVI (Figure S4Y). Mg^{2+}-induced formation of at least partial inter-domain interactions are inferred for 7 additional LSU domain pairs (Table S5). Only two domain pairs that interact in the assembled LSU are not inferred to interact at all in the rRNA/Mg^{2+} state: DI/DV and DIV/DVI. In both cases, specific rProteins contact the disparate regions that interact natively; bL28 mediates the interaction of DI/DV rRNA, and bL19 mediates interaction of DIV/DVI. These may represent late or otherwise less crucial steps in the overall assembly of the LSU.

Tertiary interactions

In the rRNA-Mg^{2+} state, tertiary interactions not supported by correlation of ΔMg^{2+} sites to assembled LSU-interacting regions must fall into one of three classes; i) already present in Na^{+}, ii) present only in Na^{+}/Mg^{2+}, but undetectable by comparative SHAPE, or iii) absent or unstable in Na^{+}/Mg^{2+}, in which case their formation is dependent on agents other than or in addition to Mg^{2+}. Given the extent and wide distribution of observed ΔMg^{2+} sites, it is unlikely that long-range inter-domain interactions would be formed in absence of Mg^{2+}. Based on this reasoning, long-range interactions for which we have no supporting evidence must fall into either class ‘ii’ or ‘iii’. In the interests of caution, we do not assume formation of any interactions not supported by interpretation of ΔMg^{2+} sites as being induced by tertiary interaction formation.

Table S5: Long-range inter-domain interactions observed in the assembled LSU, colored by their inferred status in the rRNA-Mg^{2+} state[a]

D	VI	V	IV	III	II	I
0	H61/H96 H61/H100 H73/H100	H61/H92		H26a/H49a H26a/H50	H26a/H35 H35/H73 H42/H72 H25a/H39 H40/H72 H35/H73	
I		H11/H74 H21/H75		H8/H52 H9/H51	H4/H46 H11/H32 H20/H46 H2/H26 H3/H46 H4/H46 H13/H28 H23/H32 H23/H35a H23/H31 H25/H46 H25/H40	
II	H57/H96 H41/H97	H38/H81 H42/H89 H42/H90 H37/H74 H39/H80 H39/H81 H39/H88 H39/H89 H42/H89 H29/H88 H39/H74 H42/H74	H35/H65 H33/H65 H34/H65 H35a/H65	H35/H56 H33/H52		
III						
IV	H63/H101	H68/H75 H71/H92				
V	H91/H95 H91/H97					

[a]Green shading indicates long-range inter-domain interactions inferred in the rRNA-Mg^{2+} state. Yellow shading indicates native interactions that are not seen to be present in the rRNA-Mg^{2+} state, but may be pre-organized for protein-mediated interaction (see Table S6 below). Red shading indicates native interactions not consistent with the interactions inferred in the rRNA-Mg^{2+} state, with no implied pre-organizing interactions. Helix numbers are used, though in some cases the interacting regions may be located in nearby non-helical regions.

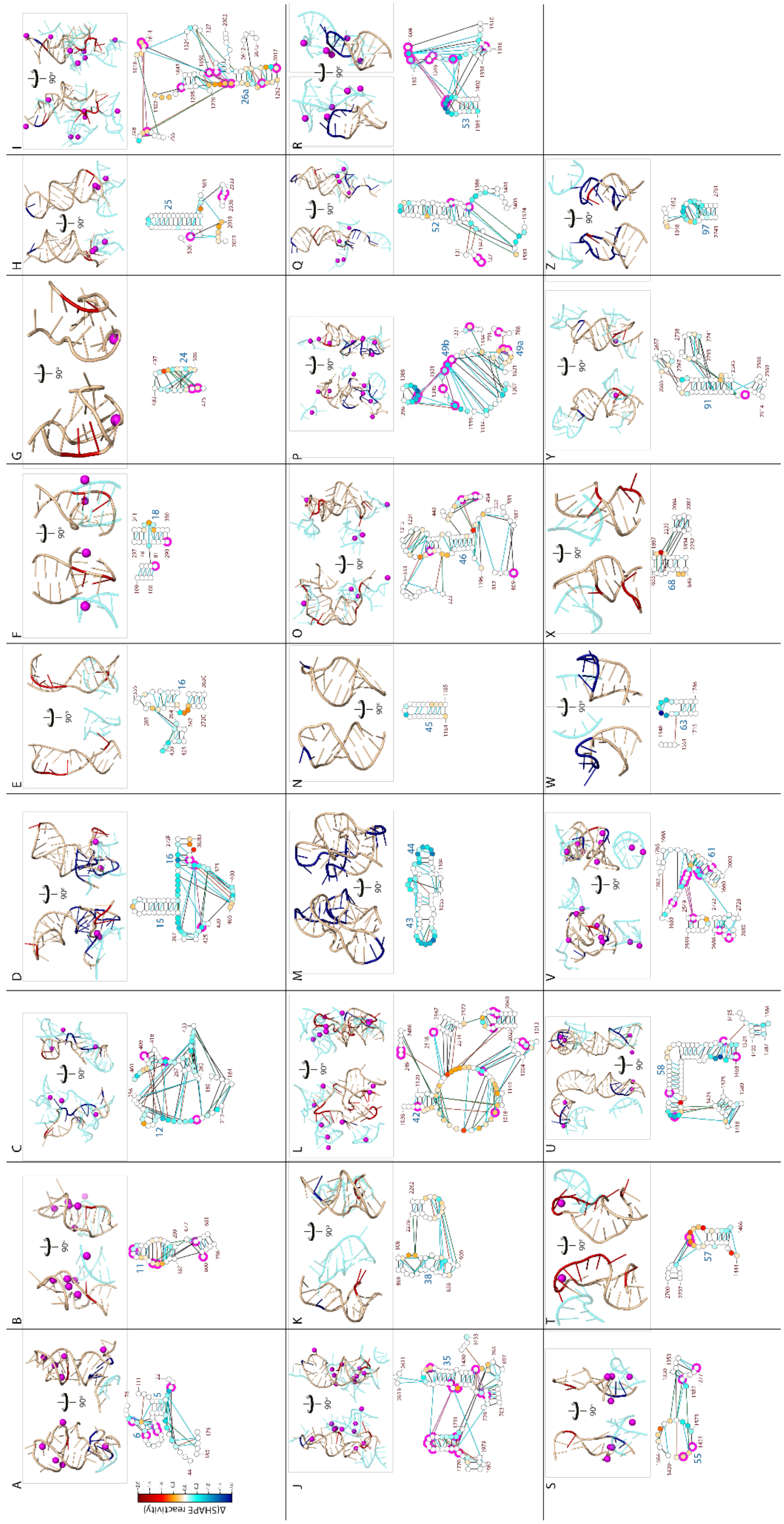

Figure S4. ΔMg^{2+} regions of the LSU rRNA. Selected regions of LSU rRNA with high densities of ΔMg^{2+} sites are shown with regions of rRNA that interact at or near the ΔMg^{2+} sites. Top Panels: 3D structure of selected regions of LSU rRNA from the *T. thermophilus* ribosome crystal structure (PDB IDs: 2J00 and 2J01). Nucleotides are colored by ΔMg^{2+} values (red, increased reactivity; dark blue, decreased reactivity; wheat, little to no change in reactivity). LSU rRNA segments that interact at or near ΔMg^{2+} sites of main helix are colored translucent cyan. Mg^{2+} cations in first shell contact with the displayed RNA (2.4 Å cut-off) are represented by magenta spheres. RNA is displayed with PyMol in cartoon representation. Bottom Panels: Mg^{2+}-induced changes in SHAPE reactivity mapped onto LSU rRNA secondary structure. Nucleotides are represented as circles, colored as in Figure 1. Lines represent RNA-RNA interactions observed in the *T. thermophilus* ribosome crystal structure (PDB 2J01), as determined by FR3D (black, base-base; orange, base-phosphate; blue, base-stacking; and green, base-sugar). Underlaid magenta circles indicate nucleotides observed to interact directly with Mg^{2+} ions. Same nucleotides are displayed in corresponding 3D and 2D representations. All samples contained 200 mM NaOAc, 50 mM NaHEPES, pH 8. Helix and nucleotide numbers are indicated.

Table S6: LSU long-range inter-domain interactions not inferred in the rRNA-Mg^{2+} state and nearby detected inferred inter-domain interactions that could pre-organize natively interacting regions for mediation by rProteins

	Interaction(s) not supported in the rRNA-Mg^{2+} state[a]	Nearby inferred interaction[a]	Figure	Mediating/stabilizing agent
D0-DII	H25a/H39 H40/H72	H42/H72	S4L	bL20 bL20
	H35/H73	H35/H73	S4J	uL3
D0-DVI	H61/H100	H61/H96	S4V	uL3/uL4/bL17
	H73/H100	H91/H97	S4Y	uL3
DI-DII	H2/H26 H3/H46 H4/H46	H4/H46	S4O	bL20 bL20 uL4/bL20
	H13/H28 H23/H32 H23/H35a	H11/H32	S4B	uL15 uL4/bL34 bL34
DI-DIII	H9/H51	H8/H52	S4Q	uL23
DII-DIV	H33/H65 H34/H65 H35a/H65	H35/65	S4J	uL2 uL2 uL2
DII-DV	H37/H74 H39/H80 H39/H81 H39/H88 H39/H89	H38/H81	S4K	uL15 uL16 uL16 uL15 uL16
	H42/H89	H42/H89&H90	S4L	uL16

[a]Helix numbers are used, though in some cases the interacting regions may be located in nearby non-helical regions.

Several sets of tertiary interactions are observed between DII and DIV in the assembled ribosome for which evidence is not found in the rRNA-Mg^{2+} state by comparative SHAPE. The unsupported DII/DIV interactions involve nucleotides in or near H65 and several helices near H35 in secondary structure (Table S6). Our data suggests Mg^{2+}-induced formation of a long range interaction between DII/DIV in the rRNA-Mg^{2+} state, involving H35 and H65 (Figure S4J), the formation of which would undoubtedly bring nearby regions involved in the remaining DII/DIV interactions into much closer proximity in 3D. Using RiboVision to map locations where each rProtein contacts rRNA in the assembled LSU,[8] it is observed that rProtein uL2 contacts rRNA at or near nucleotides involved in all of the DII/DIV interactions that are not implied in the rRNA-Mg^{2+} state. The inferred inter-domain interaction between H35/H65 may pre-organize DII and DIV such that, if uL2 were present, it could mediate and/or stabilize nearby RNA/RNA interactions. Similar cases can be made for a majority of native tertiary interactions that are not inferred in the rRNA-Mg^{2+} state (Table S6); interactions between DII/DV are pre-organized by data-supported interactions between H38/H81 (Figure S4K), H42/H89, or H42/H90 (Figure S4L) for protein-mediated interaction by uL15 or uL16, interactions between DI/DIII are pre-organized by the data-supported interaction between H8/H52 (Figure S4Q) for protein-mediated interaction by uL23, etc.

Our results for the LSU rRNA describe the use of SHAPE to support formation of specific Mg^{2+}-induced tertiary interactions in a system >10x times larger than prior studies.[9-11] Previously we performed similar Mg^{2+}-dependent SHAPE experiments with two isolated subsets of *T. thermophilus* LSU rRNA: a 615 nt model ancestral LSU rRNA[12] and DIII rRNA,[1] both prepared by *in vitro*-transcription. The observations presented here are consistent with those previous results, in which smaller rRNA systems adopt monovalent cation-induced secondary structures in agreement with established structure, and exhibit Mg^{2+}-dependent structural effects.[1,12]

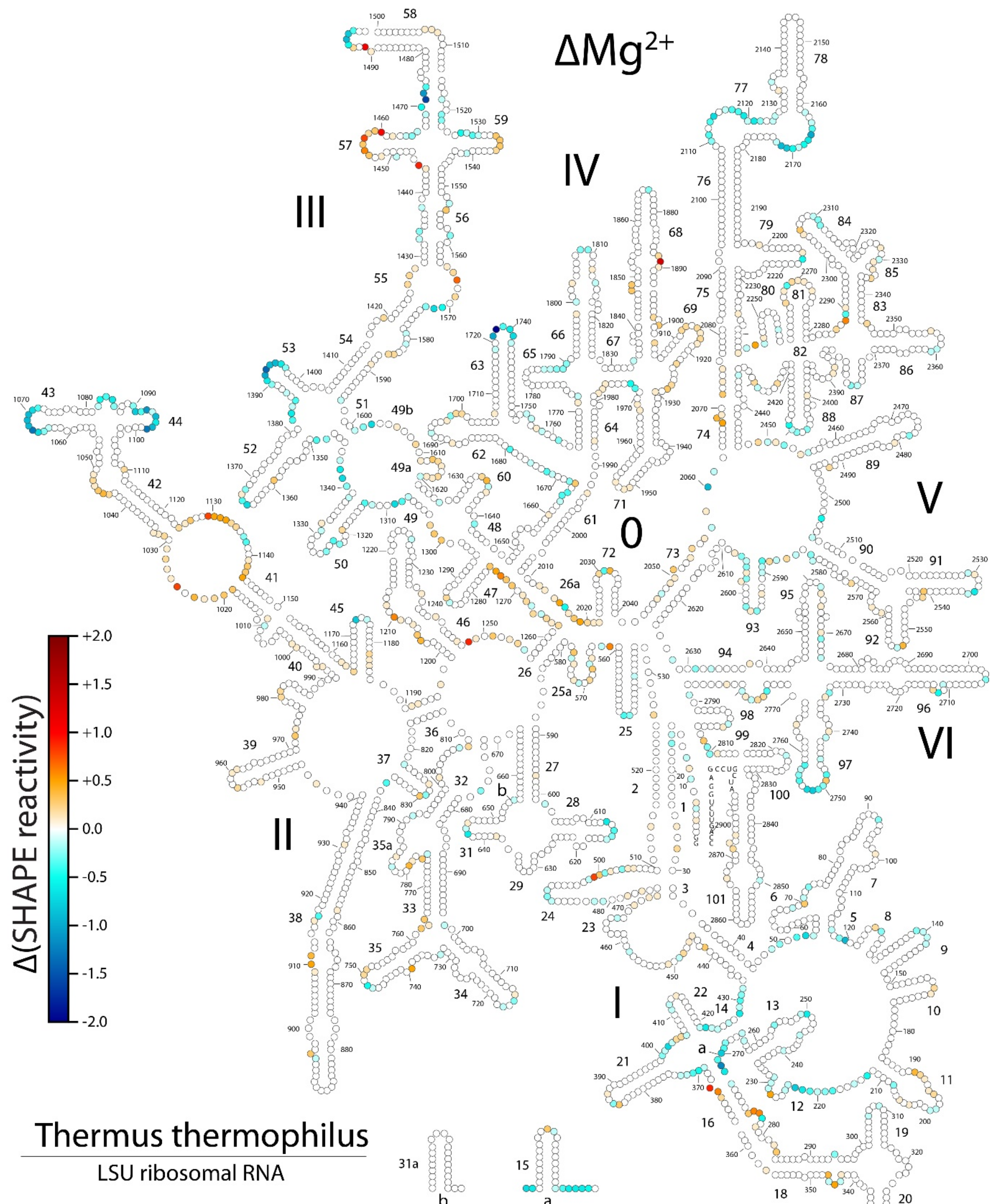

ΔMg2+
I
II
III
IV
V
VI
0
+2.0
+1.5
+1.0
+0.5
0.0
-0.5
-1.0
-1.5
-2.0
Δ(SHAPE reactivity)
Thermus thermophilus
LSU ribosomal RNA

Figure S5. Mg^{2+}-dependent structural changes in *T. thermophilus* LSU rRNA. Mg^{2+}-induced changes in SHAPE reactivity are mapped onto LSU rRNA secondary structure, compared against data obtained in presence of Na^{+} only. ΔMg^{2+} value for each nucleotide is indicated by colored circles. Positive values indicate nucleotides with increased SHAPE reactivity in presence of 10 mM Mg^{2+} and negative values denote decreased reactivity. Regions where SHAPE data is not available in at least one data set (5' and 3' ends) are displayed as sequence only. Nucleotide numbers are indicated every ~10 nt (*E. coli* numbering). Helix numbers (blue), domain numbers, and insertion points are indicated. Figure generated with RiboVision. Figure S5 is a larger, slightly modified representation of the data represented in Figure 1.

References

1. S. S. Athavale, J. J. Gossett, C. Hsiao, J. C. Bowman, E. O'Neill, E. Hershkovitz, T. Preeprem, N. V. Hud, R. M. Wartell, S. C. Harvey and L. D. Williams, *RNA*, 2012, **18**, 752-758.
2. C. D. Okafor, K. A. Lanier, A. S. Petrov, S. S. Athavale, J. C. Bowman, N. V. Hud and L. D. Williams, *Nucleic Acids Res.*, 2017, **45**, 3634-3642.
3. C. Hsiao, I.-C. Chou, C. D. Okafor, J. C. Bowman, E. B. O'Neill, S. S. Athavale, A. S. Petrov, N. V. Hud, R. M. Wartell, S. C. Harvey and L. D. Williams, *Nat. Chem.*, 2013, **5**, 525-528.
4. S. S. Athavale, J. J. Gossett, J. C. Bowman, N. V. Hud, L. D. Williams and S. C. Harvey, *PloS one*, 2013, **8**, e54384.
5. A. Liiv and M. O'Connor, *J Biol Chem*, 2006, **281**, 29850-29862.
6. C. Hsiao, S. Mohan, B. K. Kalahar and L. D. Williams, *Mol. Biol. Evol.*, 2009, **26**, 2415-2425.
7. D. J. Klein, P. B. Moore and T. A. Steitz, *RNA*, 2004, **10**, 1366-1379.
8. C. Bernier, A. S. Petrov, C. Waterbury, J. Jett, F. Li, L. E. Freil, b. Xiong, L. Wang, A. Le, B. L. Milhouse, E. Hershkovitz, M. Grover, Y. Xue, C. Hsiao, J. C. Bowman, S. C. Harvey, J. Z. Wartel and L. D. Williams, *Faraday Discuss*, 2014, **169**, 195-207.
9. S. A. Mortimer and K. M. Weeks, *J. Am. Chem. Soc.*, 2007, **129**, 4144-4145.
10. C. E. Dann, 3rd, C. A. Wakeman, C. L. Sieling, S. C. Baker, I. Irnov and W. C. Winkler, *Cell*, 2007, **130**, 878-892.
11. S. Blouin, R. Chinnappan and D. A. Lafontaine, *Nucleic Acids Res.*, 2011, **39**, 3373-3387.
12. C. Hsiao, T. K. Lenz, J. K. Peters, P. Y. Fang, D. M. Schneider, E. J. Anderson, T. Preeprem, J. C. Bowman, E. B. O'Neill, L. Lie, S. S. Athavale, J. J. Gossett, C. Trippe, J. Murray, A. S. Petrov, R. M. Wartell, S. C. Harvey, N. V. Hud and L. D. Williams, *Nucleic Acids Res.*, 2013, **41**, 3373-3385.